

Shape reconstruction and subsequent deformation of soleus muscle models using B-spline solid primitives.

Victor Ng-Thow-Hing^a, Anne Agur^b, Kevin Ball^c, Eugene Fiume^a, and Nancy McKee^d

^aDepartment of Computer Science, University of Toronto, Toronto, Canada

^bDepartment of Anatomy and Cell Biology, University of Toronto,

^cSchool of Physical and Health Education, University of Toronto,

^dDepartment of Surgery, University of Toronto

ABSTRACT

We introduce a mathematical primitive called the B-spline solid that can be used to create deformable models of muscle shape. B-spline solids can be used to model skeletal muscle for the purpose of building a data library of reusable, deformable muscles that are reconstructed from actual muscle data. Algorithms are provided for minimizing shape distortions that may be caused when fitting discrete sampled data to a continuous B-spline solid model. Visible Human image data provides a good indication of the perimeter of a muscle, but is not suitable for providing internal muscle fiber bundle arrangements which are important for physical simulation of muscle function. To obtain these fiber bundle orientations, we obtain 3-D muscle fiber bundle coordinates by triangulating optical images taken from three different camera views of serially dissected human soleus specimens. B-spline solids are represented as mathematical three-dimensional vector functions which can parameterize an enclosed volume as well as its boundary surface. They are based on B-spline basis functions, allowing local deformations via adjustable control points and smooth continuity of shape. After the B-spline solid muscle model is fitted with its external surface and internal volume arrangements, we can subsequently deform its shape to allow simulation of animated muscle tissue.

Keywords: deformable models, B-spline solids, soleus, muscle modeling

1. INTRODUCTION

The emergence of imaging techniques such as computer tomography (CT) and magnetic resonance imaging (MRI) combined with the use of computer graphics has provided researchers and practitioners with the ability to study and view anatomy in novel ways. Using images from the Visible Human data set,¹ it is possible to perform volume reconstructions of anatomic structures throughout the human body. Although we can navigate around the models of reconstructed anatomy, they are often static and cannot be deformed. To simulate living tissue, researchers have started using Visible Human data to transform static images into dynamic structures to perform virtual tasks such as facial surgery.²

However, there are cases where the inherent representation of the human body into a set of axial (transverse) slices of fixed orientation makes it difficult or impossible to extract structural information that is required for functional studies of various tissue. For example, it is difficult to identify and track individual muscle fiber bundles to determine their orientations due to the lack of continuity cues between adjacent image slices. In addition, the image resolution of the Visible Human data set is not high enough to retrieve finer structural details of individual muscle fiber bundles. Muscle fiber orientation is important for calculating force generation, visualizing shape changes, and understanding the role of skeletal muscles in the creation of human movement.

The architecture of a muscle consists of its external configuration and dimensions, and the internal arrangement and morphology of its contractile elements. Grossly, skeletal muscle has been described as being parallel, circular or

Other author information:

V.N.: E-mail: victorn@dgpc.toronto.edu

A.A.: E-mail: anne.agur@utoronto.ca

K.B.: E-mail: ball@phe.utoronto.ca

E.F.: E-mail: elf@dgpc.toronto.edu

N.M.: E-mail: n.mckee@utoronto.ca

pennate in fiber arrangement. Historically muscle architecture studies have been purely descriptive in nature, but a quantitative analysis of muscle architecture is important because the structural parameters have a profound effect on muscle function.³ Previous work has focused on the muscle as a whole with little attention being paid to different regions within a muscle. Commonly, structural parameters have been recorded as single values for the whole muscle, regardless of the complexity of pennation. Parameters measured have included muscle length, fiber length, angle of pennation etc.⁴⁻⁶ What is of great interest and has not been documented is the specific architecture of multi-pennate muscle. Knowledge of structural properties of each part of the muscle would help to establish the overall function, where function may include more sophisticated factors than simply the amount of shortening between the origin and insertion. The detailed measurement and modeling of the architectural characteristics of the soleus muscle (Figure 1) was chosen as the focus of this study, since these muscles are major contributors to human ambulatory power.

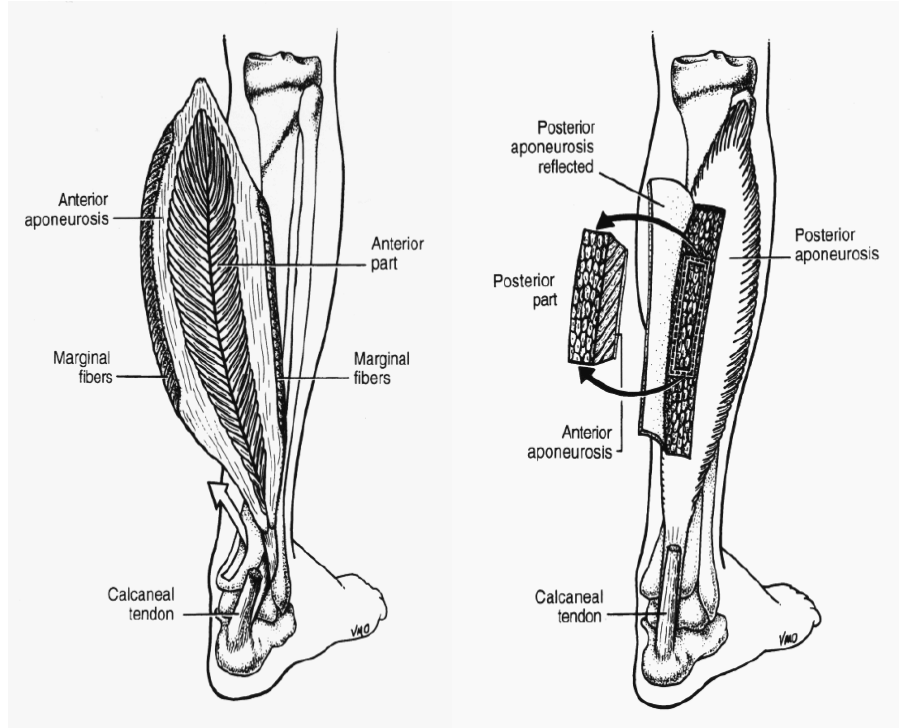


Figure 1. Marginal (M), posterior (P) and anterior (A) fibers in the soleus muscle (*illustrator Valerie Oxorn*⁷)

In creating a detailed model of muscle, there is a need to represent its smooth shape properties while simultaneously being able to specify its internal architecture. Such a model must also be capable of deformations to reproduce the shape changes that occur when active muscle contracts. We introduce B-spline solids as useful modeling primitives for skeletal muscle as well as for potentially other anatomic structures. The properties of B-spline basis functions allow local deformations in shape. A continuous solid domain can be defined with inherent smoothness properties as well as an internal coordinate system that allows parameterization of vector and scalar properties within the entire solid as well as on its boundary surface. The inherent smoothness and compactness of representation in B-spline solids make them an interesting alternative to the more faceted polygon representations that are often created using the *Marching Cubes algorithm*.⁸ Quantities like surface normals and volume can be computed directly from B-spline solids without the need for approximation.

This form of three-dimensional parameterization can also be used to nest or restrict the deformations of solids within the volume of another solid that contains it. By using B-spline solids, animation and modification of shape at interactive rates is possible. Solids can be created from a relatively sparse amount of data through the use of 3-D sampling function techniques. The mathematical formulation of B-spline solids allows them to be applicable to optimization methods that can constrain the nature of shape changes, similar to finite element techniques.⁹ We will show how B-spline solids can be used to create deformable models of soleus muscle from both the Visible Human dataset and from dissected soleus specimens. From this, we will compare the quality of the reconstructed shapes in

each case. Before describing the procedure for constructing deformable models of soleus muscle, the mathematical formulation of B-spline solids will be reviewed.

2. INTRODUCTION TO B-SPLINE SOLIDS

B-spline solids are straightforward extensions of B-spline curves and surfaces into the volumetric domain. A third parameter is added to the function to allow enumeration of points throughout a volume in addition to an iso-surface (one parameter constant) or a streamline curve (two parameters constant). Mathematically, a B-spline solid is represented by the following equation:

$$\mathbf{V}(u, v, w) = \sum_{i=0}^l \sum_{j=0}^m \sum_{k=0}^n B_i^u(u) B_j^v(v) B_k^w(w) \mathbf{C}_{ijk} \quad (1)$$

where each $\mathbf{C}_{ijk} \in \mathcal{R}^3$. The set $\mathbf{C} = \{\mathbf{C}_{ijk}\}$ of points form a control point lattice which will influence the shape of the B-spline solid (Figure 2A). \mathbf{V} describes a parametric solid given by the tritensor product of these B-spline basis functions (in this case, the polynomials $B_i^u(u), B_j^v(v), B_k^w(w)$) with the control points in \mathbf{C} . We can substitute the control points \mathbf{C} with other vector or scalar values to define other continuous fields or functions within the solid such as continuous internal forces. The basis functions for each parameter need not all have the same order and each basis function family is indexed depending on the size of its associated knot vector, U, V or W . The knot vectors form a sequence of points that partitions the parameter domain space, determining the local region of influence for each basis function. As each control point is weighted with B-spline basis functions, moving a point will deform a region of the solid as dictated by the shape of the B-spline basis functions which are in turn determined by the knot vectors (see Figure 2). For a more detailed description of the properties and evaluation of B-spline basis functions, please refer to Hoschek and Lasser.⁹

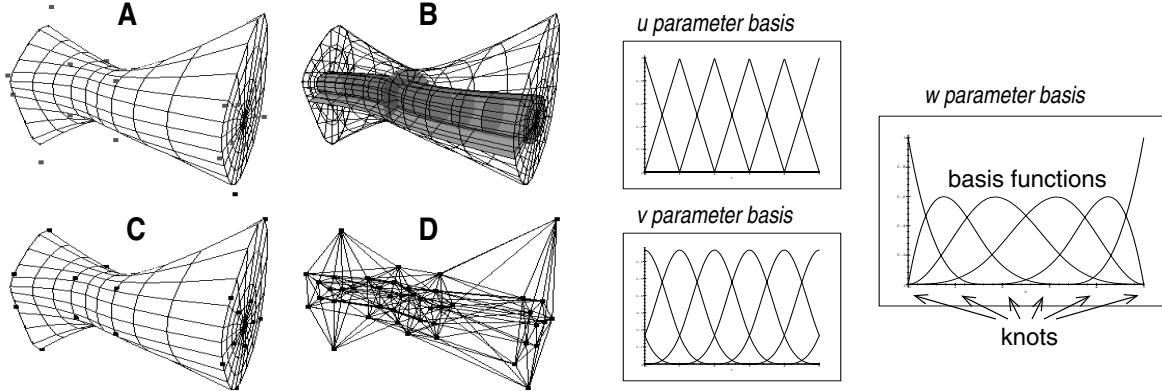


Figure 2. Features of B-spline solids. (A) B-spline solid with control points. (B) Iso-parametric surfaces of a B-spline solid. (C) B-spline solid with sample points. (D) Sample points are connected with a viscoelastic network. On the right, the uniform basis functions for the u, v , and w parameters of a B-spline solid are displayed.

2.1. Control point lattice design

The control point lattice determines the shape of the B-spline object. The coordinate system used to represent and position control points will determine the space in which the object will be displayed. Although any three-dimensional coordinate system can be used for solids, we chose the cartesian coordinate system to represent geometry for 3-D graphics.

The topology of the lattice defines the topology and the control point indexing of its associated B-spline solid. Therefore, the design of the control point lattice is influential in creating the user interface handles that can be used to modify the object's shape.¹⁰ The indexing of control points will affect the interpretation of the solid's iso-parametric surfaces or curves when one or more parameters is held constant (see Figure 2B).

The choice of a control point lattice depends on the type of object that is being modeled. We chose a natural cylindrical indexing that allowed us to retain the basic cylindrical topology of muscle-like bundles after shape deformation. The topology of a cylindrical lattice is actually the same as that of a tube since it includes outer and inner surfaces, with the main axis corresponding to the inner surface where all the surface points are coincident on the axis curve (see Figure 3).

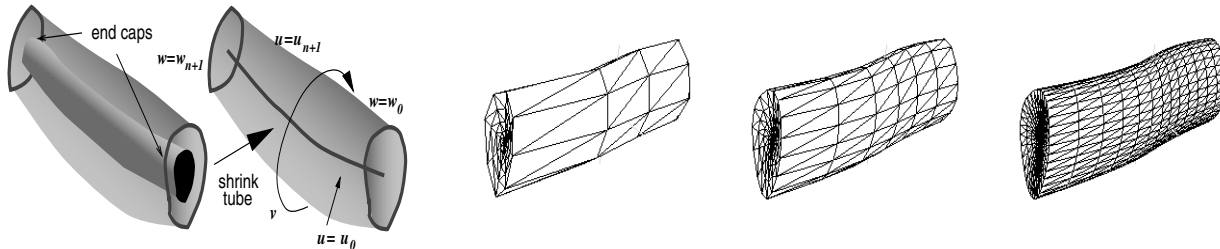


Figure 3. Left: The parameterization of the cylindrical B-spline solid. The topology of the solid is actually the same as a tube. Right: B-spline solids can be retessellated to any desired level of detail.

2.2. Interactive display of B-spline solids

For the purposes of animation, we need to quickly display and update the changing shape of B-spline solids. A key advantage of using a solid formulation instead of a surface parameterization is that the solid produces a unified model that allows us the flexibility of displaying arbitrary iso-surfaces within the solid. It is possible to display subvolumes within the solid (Figure 2B) by displaying different iso-parametric surfaces. To visualize the closed outer surface of the solid, we simply draw iso-parametric surfaces (holding one parameter constant while varying the other two over their respective domains) that correspond to the boundary of the parameter domains. Although it is possible to create a closed cylindrical surface with a single B-spline surface, duplicate control points or additional knots must be inserted to create discontinuities at the edges between the caps and the outer shell of the cylindrical shape.

Due to the use of multiple knots in the u and w parameter domains, the external control points are solely responsible for the shape of the solid's boundary since the internal basis functions evaluate to zero at the boundaries. Consequently, the outer surface of a B-spline solid is equivalent to a standard B-spline surface,⁹ making it possible to apply standard acceleration techniques to interactively update and display B-spline solids. To take advantage of graphics hardware, it is necessary to tessellate the B-spline solid surfaces. By pre-evaluating the B-spline basis functions at tessellation points and storing these basis function values in a table, we can quickly update a pre-existing tessellation whenever a control point is changed. A given control point will affect only a finite set of tessellation points which correspond to the parameter values of u, v , and w where $B_i^u(u)B_j^v(v)B_k^w(w) \neq 0$ for a control point \mathbf{C}_{ijk} . By storing the non-zero $B_i^u(u)B_j^v(v)B_k^w(w)$ for each control point, we can achieve fast incremental updates of the solid deformations at interactive rates. Choosing the density of tessellation points allows us to produce different levels of detail of each model (Figure 3), which will be needed to display very complex scenes with hundreds of these solids in them.

3. METHODS AND MATERIALS

The process of producing deformable models of soleus muscle from various sources of data can be divided into several stages:

1. 3-D data is obtained from the Visible Human data set and from serially dissected human soleus specimens.
2. From the sampled data, a *continuous volume sampling function* (CVSF) is built which has a domain consisting of three parameters $(\tilde{u}, \tilde{v}, \tilde{w}) \in [0, 1]^3$. The parameter space maps to a continuous volume that approximates the volume of the anatomic structure with the characteristic that the volume intersects the original data that was used to build the function. During the construction of this function, steps can be taken to produce evenly distributed samples.

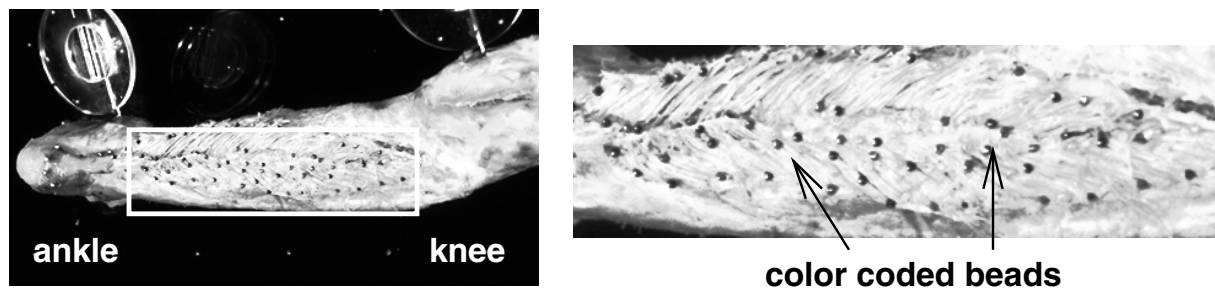


Figure 4. Dissection of anterior soleus (inside the rectangle). The fiber bundles are pinned with color-coded beads and the specimen with marker clusters is placed on the base plate.

3. Once the CVSF is available, samples can be freely selected and used in a data-fitting process with a B-spline solid that guarantees intersection of the sample points. Samples are chosen both on the surface and in the interior of the solid.
4. Having obtained a B-spline solid approximation of the muscle, we can perform volume visualizations of muscle fiber orientations, or subsequently deform the shape for simulation or user adjustment purposes.

We will now discuss each of these stages in more detail.

3.1. Obtaining 3-D data from anatomical specimens

3.1.1. Visible Human data

We obtained a subset of images of soleus muscle from the Visible Human Male data set. To avoid managing the large amount of data, we used lower resolution 24 bit images at 800x500 (MRI data is 256x256 and CT is 512x512)¹ resolution instead of the original axial images of 2048x1216. Every tenth slice (intervals of 1cm) was used in a sequence of images bounding the posterior and anterior soleus of the right leg.

As we could not reliably segment the individual posterior and anterior regions of the soleus by automatic means, an anatomist examined each of the data images and delineated the different regions, outlining the boundaries using a dark thick line with an image paint program. This facilitated the use of active contours (“snakes”)¹¹ to quickly guide a deformable contour curve to the marked boundaries. From the active contour software, we were able to obtain two sets of contour curves, made up of a sequence of 3-D coordinates, for each of the posterior and anterior soleus. The contour curves for each set had the same number of points, allowing one-to-one mappings between the points on the adjacent contours.

3.1.2. Dissected soleus specimens

The human soleus muscle has three parts: *posterior, marginal and anterior*¹² (Figure 1). To develop the model, the soleus muscle, located in situ, was serially dissected from posterior to anterior. At each level the beginning and end of 50-100 representative fiber bundles distributed throughout the muscle volume were identified and pinned with color coded beads. The specimen was placed on a calibrated base plate and photographs were taken at each level of the serial dissection using three 35mm cameras that were calibrated using the *direct linear transformation* (DLT)¹³ (Figure 4). These images were transferred to CD-ROM and the locations of the beads digitized. Visible in each image were two rigid objects of known dimensions. These objects were attached directly to the bones of the specimen. Reference points on these objects were digitized and rigid body procedures were used,^{14,15} on a level by level basis, to achieve a consistent alignment of all of the 3-D coordinates that were viewed across the muscle’s dissected surface. These muscle-related coordinates were ordered to generate line segments that represented the fiber orientations. This entire procedure will be referred to as *anatomical photogrammetry*. Plots of the muscle in whole and in part were created to observe and verify the architecture seen in the cadaveric specimen.

3.2. Constructing the continuous volume sampling function

We needed to develop two different approaches to create *continuous volume sampling functions* (CVSFs) for the Visible Human and dissected soleus data sets. The form of the CVSF is:

$$CVSF(\tilde{u}, \tilde{v}, \tilde{w}) = \mathbf{s}_{\tilde{u}\tilde{v}\tilde{w}} \quad (2)$$

where the three parameters $(\tilde{u}, \tilde{v}, \tilde{w}) \in [0, 1]^3$. This allows a relatively sparse amount of data to be used to specify the shape of a B-spline solid as the *CVSF* will interpolate between the given data. A sample point, $\mathbf{s}_{\tilde{u}\tilde{v}\tilde{w}}$, is a 3-D point that can be chosen anywhere within the continuous volume defined by the *CVSF* using the parameters $(\tilde{u}, \tilde{v}, \tilde{w})$. Sample points are used for defining the B-spline solid's shape during the data-fitting process.

3.2.1. Visible Human

The Visible Human data produced a set of contour curves for an individual muscle where each contour curve is an ordered set of points that make up a closed polygon. This data was obtained directly from the active contour image processing program we used. The contours belonging to a common set were re-indexed by offsetting the ordering to minimize the least squared distance between adjacent points sharing the same index. This helped to reduce twisting distortions in shape along the muscle axis. We chose the parameter \tilde{u} to correspond roughly to the radial distance formed by the centroid axis of the contours, \tilde{v} to span a distance around the circumference of the axis and \tilde{w} to represent the fractional length along the longitudinal axis of the muscle (Figure 5). To retrieve a given sample point, we first create an interpolating spline, $\mathbf{c}_i(\tilde{v}), i = 0, 1, \dots, n$, for each of the $n + 1$ contour curves making up a muscle. Arc length parameterization is used to obtain a point at the fractional distance \tilde{v} around the circumference of each of the contours. Another interpolating B-spline, \mathbf{l} , is used that consists of the sequence of points $\mathbf{c}_i(\tilde{v})$ that are chosen from each of the $n + 1$ contours. A point $\mathbf{l}(\tilde{w})$ is evaluated that corresponds to the fractional length \tilde{w} along the spline curve \mathbf{l} . A second point $\mathbf{a}(\tilde{w})$ was taken that coincided with the fractional length \tilde{w} along an interpolating spline made up of the centroids of each axis.

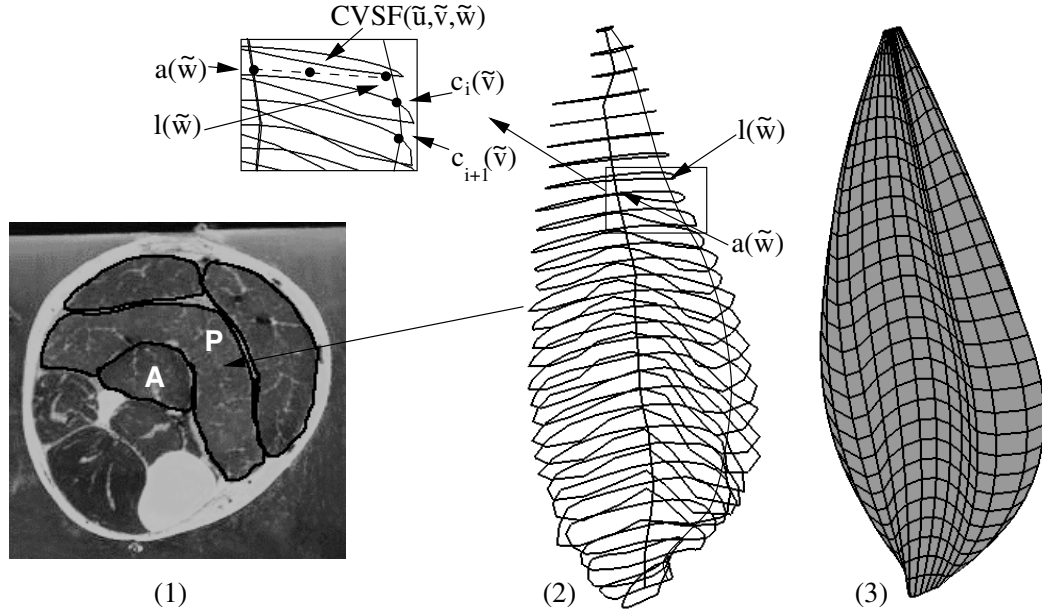


Figure 5. Stages of data fitting for Visible Human data. (1) Contours of the posterior (P) and anterior (A) soleus are extracted from images. (2) CVSF is built to generate sample points (only posterior contours are shown). (3) B-spline solid is generated to intersect the sample points.

Second degree interpolating curves were used to create a C^1 continuous volume shape. Higher degree splines introduced unwanted oscillations in shape and were more expensive to compute. The final desired sample points $\mathbf{s}_{\tilde{u}\tilde{v}\tilde{w}}$ were obtained by linear interpolation between $\mathbf{l}(\tilde{w})$ and $\mathbf{a}(\tilde{w})$ (Figure 5). Higher-order interpolation schemes could be applied by using more sample points in the interior of the solid, but we found that linear interpolation produces an even distribution of fibers in the solid.

3.2.2. Dissected soleus

We developed a method of constructing the CVSF from a series of profile curves that follow the edges formed by the ends of the line segments that were retrieved using anatomic photogrammetry. By parameterizing profile curves so that the same parameter in two curves produces the end points of the same line segment, we guarantee that muscle fiber bundle orientations are preserved. The CVSF volume is formed by interpolating or sweeping between the profile curves. For example, if we are given two end cap curves and an axis curve that outline a cylindrical shape (Figure 3), the swept volume creating the CVSF is computed as:

$$\mathbf{CVSF}(\tilde{u}, \tilde{v}, \tilde{w}) = (1 - \tilde{u})\mathbf{axis}(\tilde{w}) + \tilde{u}[(1 - \tilde{w})\mathbf{cap}_1(\tilde{v}) + \tilde{w}\mathbf{cap}_2(\tilde{v})]. \quad (3)$$

We illustrate the method by showing the CVSFs developed for marginal (M), posterior (P) and anterior (A) soleus regions in Figure 6.

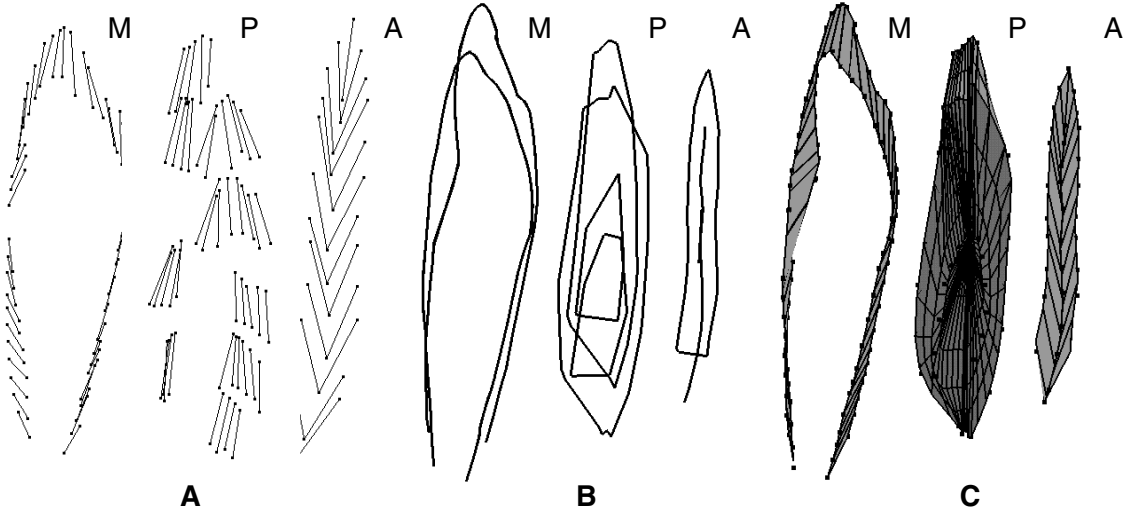


Figure 6. Creating the CVSF with profile curves. (A) 3-D points and line-segments are retrieved from soleus using anatomical photogrammetry. (B) Profile curves are created to define the CVSF. (C) The resulting B-spline solids with the sample points used to define its shape.

3.3. Fitting the data to the B-spline solid shape

With the creation of the continuous function **CVSF**, we are free to sample any number of points anywhere within the domain of **CVSF**. However, we restrict the number of samples we wish to take to be equal to the number of degrees of freedom (control points) in our B-spline solid. This allows us to create a set of linear systems through which we can solve for the control points efficiently. In contrast to Hsu *et al.*,¹⁶ who developed a general direct manipulation interface for any point within a free form deformation lattice, we restrict manipulation to the original sample points used for data fitting.

The control points cannot all be solved for in a single large linear system containing the sample points. This is because linear dependencies arise due to multiple knot vectors occurring at the boundaries of the B-spline solid's knot vectors. For example, the control points around the outer ring of an end cap of a cylindrical B-spline solid is sufficient to completely specify the shape of the cap's boundary. Including these control points in a larger linear system would over-constrain the problem and create a singular matrix. The solution is to solve a sequence of linear systems that partition the unknown control points into solvable sets. The boundary conditions of the solid are solved first. These boundary control points can then be used to solve for the internal control points within the solid. Figure 7 illustrates the sequence that the various sets of control points must be solved in. The general form of these linear systems is:

$$\mathbf{Bc} = \mathbf{s} - \mathbf{b} \quad (4)$$

where **c** are the control point components to solve, **s** are the sample points to fit, and **B** is a matrix where each row is made up of the evaluated basis functions at the parameter values assigned to the sample point stored in the same row

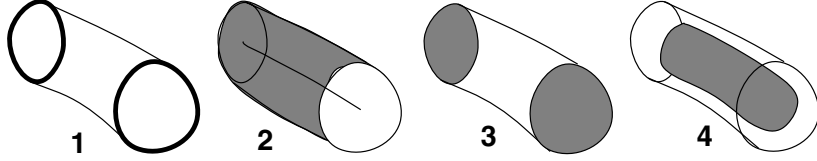


Figure 7. Proper sequence for solving all the control points for a B-spline solid. 1. Cap rings. 2. Outer shell and inner axis. 3. Inner caps. 4. Remaining region between the outer shell, axis and caps.

of \mathbf{s} . In cases where the boundary control points have been solved, \mathbf{b} will store the product of these solved control points and their corresponding evaluated basis functions which will be subtracted from \mathbf{s} to maintain an independent set of equations. In some cases, the data fitting matrices, \mathbf{B} , for two systems are identical due to symmetries in the boundary conditions of the solid. This allows us to solve two simultaneous systems in one pass. In all cases, we perform an LU factorization of the matrix \mathbf{B} and use the factors to solve two simpler linear systems with triangular matrices to significantly accelerate the solution of the linear systems.¹⁷ Since we must repetitively solve the system each time the sample points are moved, the acceleration technique is very important. These factors can be stored and reused to recompute the new control points for an animated set of sample points very quickly without the need to expensively compute inverse matrices.

The choice of sample points and their corresponding parameters within the B-spline solid determines how the shape will change as sample points are moved. We choose sample point parameters that locate the maximum of each basis function of the B-spline basis for each parameter dimension. This adjusts the weighting of control points that must be moved to interpolate the sample point so that the corresponding control point of the basis function has the greatest influence on the sample point. Forsey and Bartels¹⁸ use a similar formulation for direct manipulation of hierarchical B-spline surfaces. They avoid solving linear systems by restricting the manipulation of sample points to only one at a time.

Sample points are an effective alternative to control points because they allow the user to specify the exact placement of the solid in space. The use of sample points becomes very useful when fitting a viscoelastic system over these points instead of the control points. Spatial constraints between sample points create direct correlations between actual points in the solid. In contrast, constraints acting between control points can create undesirable deformations in the underlying solid shape.

4. RESULTS

4.1. Obtaining muscle fiber orientations

Once the B-spline model is obtained, we can visualize the iso-surfaces or streamlines within the solid. Figure 8 illustrates streamlines for B-spline solids, representing parts of the posterior and anterior soleus, extracted from both the Visible Human and dissected soleus specimens with various streamlines and iso-surfaces displayed. The Visible Human data provides a nicer overall shape definition due to the higher density of original sample points. However, the internal fiber orientations are incorrect due to the lack of internal markers within the contours to construct an accurate CVSF. In contrast, using the profile curves to create the CVSF allowed close matching of fiber end points in the dissected soleus specimens than in the Visible Human data set derived models. With the dissected soleus specimens, we were able to resolve the soleus into marginal, posterior and anterior fiber groups. This level of detail was not apparent from the Visible Human images.

4.2. Deforming B-spline solids

Control points on the original sample points of the B-spline solids can be directly manipulated to locally deform the solid shape at interactive rates. Notice that the control points may not necessarily lie on the solid's surface or within its volume (except in degree 1 B-spline solids). For direct manipulation of solids, we used the set of sample points $\mathbf{s}_{\bar{u}\bar{v}\bar{w}}$ that were used to fit the B-spline solid's shape and solved for a new configuration of control points to define the resulting shape change. For simulation, it is necessary to coordinate the movement of many control or sample points simultaneously. We are currently experimenting with two techniques: (1) a network of viscoelastic units connecting the sample points and (2) nonlinear constrained optimization techniques¹⁹ that seek to minimize energy functionals of the control points while conserving volume. It is possible for a modeler to define different

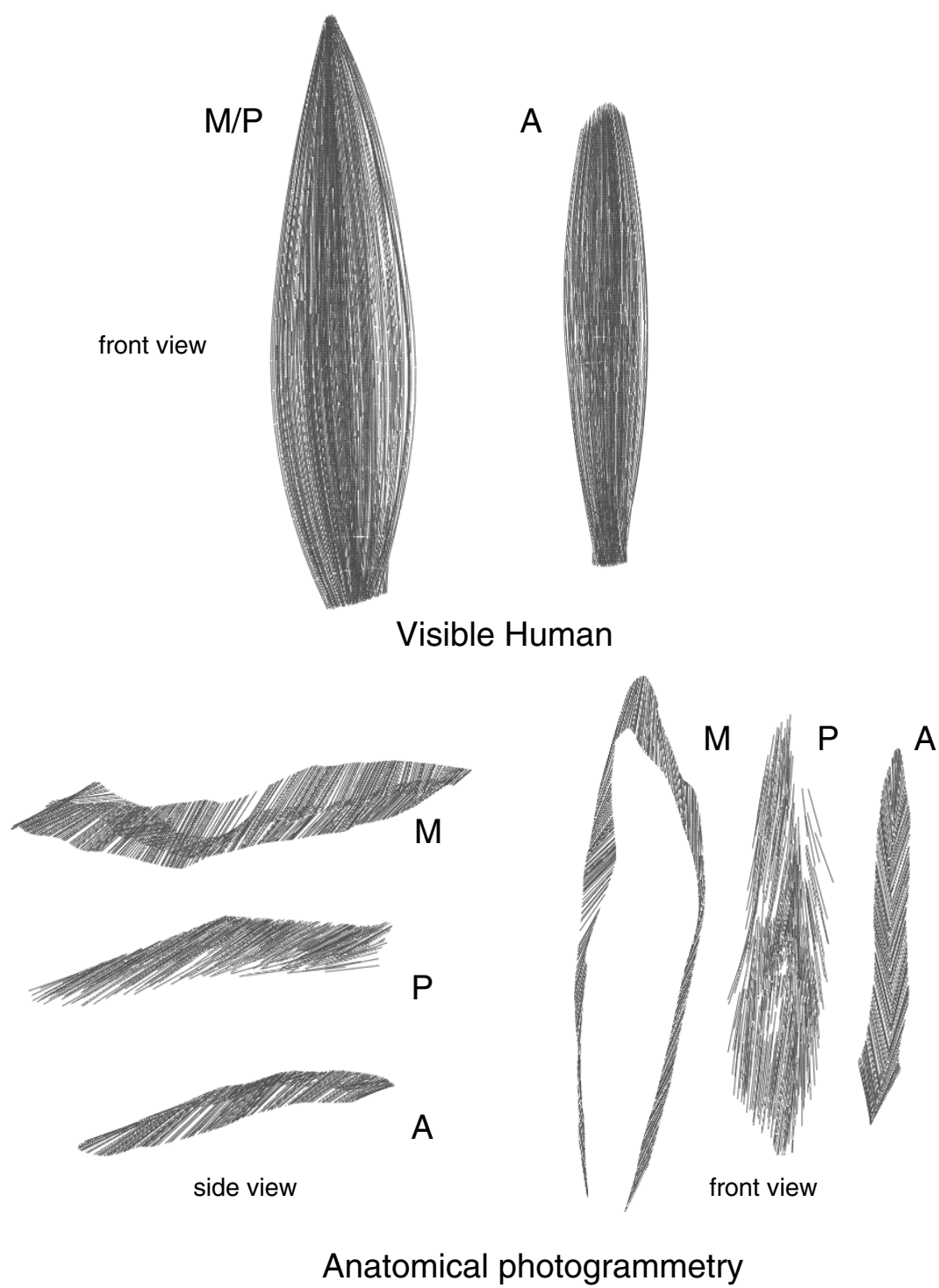


Figure 8. Fiber orientations derived from Visible Human data and serially dissected soleus. Multiple views of the fibers obtained from photogrammetry of dissected soleus show that orientations are accurately reconstructed (M=marginal fibers, P=posterior fibers, A=anterior fibers). In the Visible Human data, it is impossible to distinguish between posterior and marginal fibers. Note that the aspect ratio of the Visible Human image has been adjusted to correct for the 3:1 height to width ratio in the data set.

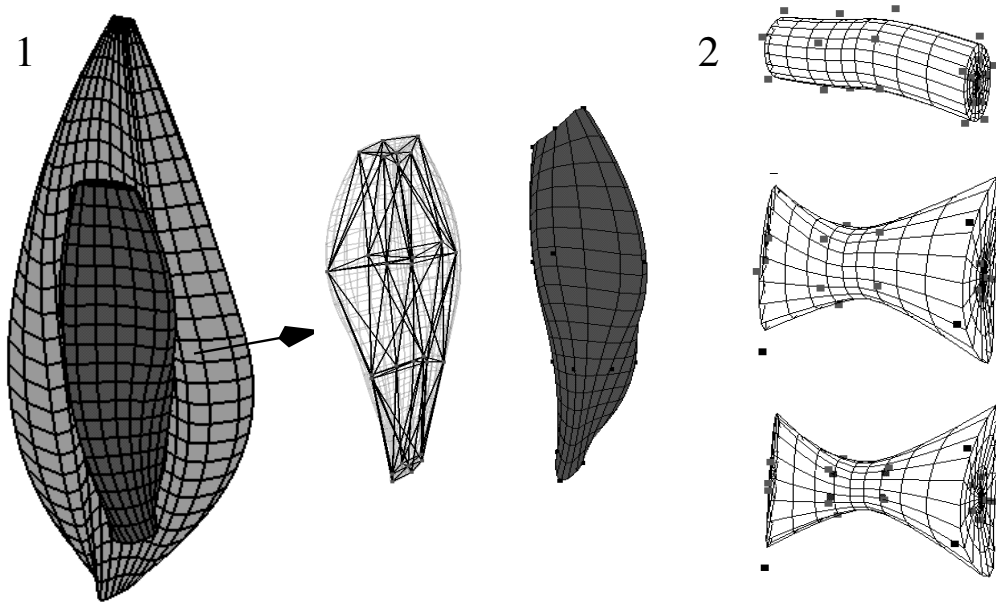


Figure 9. (1) The anterior soleus has a viscoelastic network applied to its sample points that deforms its shape. (2) The B-spline solid optimizes its least squares change in control points while conserving volume. The top shape is deformed to create the middle shape. After optimization, the bottom shape has the same volume as the top one.

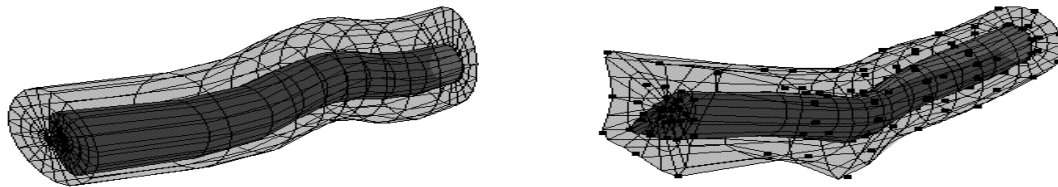


Figure 10. B-spline solids can be nested within each other to allow modeling of components within an anatomic structure. As the outer solid changes shape, the nested solid deforms with it.

stiffness or damping coefficients for the viscoelastic units, allowing nonhomogenous physical properties throughout the solid. The speed of the simulation depends on the number of sample points, the number of springs and the degree of the basis functions of the B-spline solid. For optimization, we experimented with a simple case using only control point values to minimize the least-squares distance between the control point configurations of an initial B-spline solid shape and the deformed solid while conserving volume (Figure 9). In addition, the mathematical formulation of B-spline solids can potentially be applied to finite element analysis by defining energy functionals that can be minimized to find the optimal control point configuration.

4.3. Nesting solids

The three-dimensional parameter space of a B-spline solid can be used to nest other solids within each other, similar to a technique in computer graphics called *free-form deformations*.²⁰ We used nonlinear least squares numerical techniques²¹ to solve the inverse problem of finding the parameters u, v, w for a given point that lies within a solid. If every control or sample point in a B-spline solid lies entirely within another solid, we can deform the outer solid while simultaneously deforming the solids that reside within it (Figure 10). This can be used to model substructures within anatomy. For example, fiber bundles can be modeled as individual solids residing within a larger solid that represents the envelope of outer deep fascia tissue. This technique can also be used to link solids together at common points.

5. CONCLUSIONS AND DISCUSSION

We have shown that B-spline solids can be a useful primitive for developing deformable models of skeletal muscle. Techniques have been introduced to construct continuous representations of volume from discrete data. Since B-spline solids can be defined completely with its control points and knot vectors, they can require significantly less storage than a dense set of polygons.

The three dimensional parameterization allows true volume analysis of the shapes, providing arbitrary streamline or iso-surface visualizations. In the case of streamline construction, careful design of the CVSF can provide accurate depictions of muscle fiber orientations in soleus for subsequent use in functional simulation of muscle. This was aided with the use of dissection and optical recording techniques designed solely for capturing muscle fiber orientations (anatomical photogrammetry). Although the Visible Human data is helpful for delineating gross sections of anatomy by segmenting the regions using axial boundary information, internal muscle architecture cannot be determined. The correct fiber arrangements provided from the serially dissected soleus will allow future studies to examine muscle contraction and subsequent force generation with accurate muscle pennation effects.

We hope to refine the B-spline solid model to set the stage for further research on applying B-spline solids for non-invasive surgical simulation using functional, deformable models of tissue, especially with skeletal muscles. B-spline solids can have other topologies such as tubular and ellipsoidal shapes to allow modeling of a wider variety of shapes. Nonuniform knot vectors can potentially lead to better data-fitting of solids with less sample points required or the knot vectors can be adjusted to allow greater shape control in selected regions of the solid.

We intend to continue exploring the use of viscoelastic networks in combination with volume-preserving constraints. This promises the development of faster interactive visualizations that can be used for functional studies of muscle and their role in creating movement in animals. For example, B-spline solids could be incorporated as muscle primitives in a system where they can be attached to an underlying skeleton and create active motion. Such a tool would be useful for the exploration of biological systems without the need to perform invasive procedures.

We found it exciting that this work arose out of the common interests from three different disciplines: computer animation, clinical anatomy and biomechanics. Anatomy provided the methods to perform serial dissections to categorize the different orientations of muscle fibers in the soleus. Optical triangulation techniques used in biomechanics made it possible to convert markers on muscle fibers to three dimensional points. Computer animation research drove the development of B-spline solid primitives to create deformable shapes for the muscles. Each discipline has gained from the synergies that have resulted from this co-disciplinary work.

6. ACKNOWLEDGEMENTS

This work was partially funded by NSERC, ITRC of Ontario, AO/ASIF - Foundation of Switzerland and the Department of Surgery, Faculty of Medicine, University of Toronto.

REFERENCES

1. U. N. L. of Medicine, "The visible human project." MRI, CT, and axial anatomical images of human body, October 1996.
2. R. Koch, M. Gross, F. Carls, D. von Buren, and Y. Parish, "Simulating facial surgery using finite element models," in *Computer Graphics (SIGGRAPH '96 Proceedings)*, pp. 421–428, 1996.
3. R. Woittiez, P. Huijting, and R. Rozendal, "Influence of muscle architecture on the length-force diagram: a model and its verification.," *Pflugers Arch.* **397**, pp. 73–74, 1983.
4. T. Wickiewicz, R. Roy, P. Powell, and V. Edgerton, "Muscle architecture of the human lower limb.," *Clinical Orthopaedics and Related Research* **179**, pp. 275–283, 1983.
5. J. Friederich and R. Brand, "Muscle fibre architecture in the human lower limb.," *Journal of Biomechanics* **23**, pp. 91–95, 1990.
6. G. Yamaguchi, A. Sawa, D. Moran, M. Fessler, and J. Winters, "A survey of human musculotendon actuator parameters.," in *Multiple muscle systems: Biomechanics and movement organization*, J. Winters and S. Woo, eds., pp. 717–773, New York: Springer-Verlag, 1990.
7. V. Oxorn, A. Agur, and N. McKee, "Resolving discrepancies in image research: The importance of direct observation in the illustration of the human soleus muscle.," *Journal of Biocommunication* **25**(1), 1998.

8. W. E. Lorensen and H. E. Cline, "Marching cubes: A high resolution 3D surface construction algorithm," in *Computer Graphics (SIGGRAPH '87 Proceedings)*, M. C. Stone, ed., vol. 21, pp. 163–169, July 1987.
9. J. Hoschek and D. Lasser, *Fundamentals of Computer Aided Geometric Design*, A K Peters, 1989.
10. S. Coquillart, "Extended free-form deformation: A sculpturing tool for 3D geometric modeling," in *Computer Graphics (SIGGRAPH '90 Proceedings)*, F. Baskett, ed., vol. 24, pp. 187–196, Aug. 1990.
11. M. Kass, A. Witkin, and D. Terzopoulos, "Snakes: Active contour models," *International Journal of Computer Vision* **1**(4), pp. 321–331, 1987.
12. A. Agur and N. McKee, "Soleus muscle: Fiber orientation.," *Clinical Anatomy* **10**, p. 130, 1997. Abstract.
13. Y. Abdel-Aziz and H. Karara, "Direct linear transformation into object space coordinates in close-range photogrammetry," in *Symposium on Close-Range Photogrammetry*, pp. 1–19, 1971.
14. K. Ball and M. Pierrynowski, "Estimation of six degree of freedom rigid body segment motion from two dimensional data.," *Human Movement Science* **14**, pp. 139–154, 1995.
15. K. Ball and M. Pierrynowski, "Classification of errors in locating a rigid body.," *Journal of Biomechanics* **29**, pp. 1213–1217, 1996.
16. W. M. Hsu, J. F. Hughes, and H. Kaufman, "Direct manipulation of free-form deformations," in *Computer Graphics (SIGGRAPH '92 Proceedings)*, vol. 26, pp. 177–184, 1992.
17. W. H. Press, S. A. Teukolsky, W. T. Vetterling, and B. P. Flannery, *Numerical Recipes in C*, Cambridge University Press, second ed., 1992.
18. D. R. Forsey and R. H. Bartels, "Hierarchical B-spline refinement," in *Computer Graphics (SIGGRAPH '88 Proceedings)*, J. Dill, ed., vol. 22, pp. 205–212, Aug. 1988.
19. P. E. Gill, W. Murray, and M. H. Wright, *Practical Optimization*, Academic Press, 1981.
20. T. W. Sederberg and S. R. Parry, "Free-form deformation of solid geometric models," in *Computer Graphics (SIGGRAPH '86 Proceedings)*, D. C. Evans and R. J. Athay, eds., vol. 20, pp. 151–160, August 1986.
21. V. Ng-Thow-Hing and E. Fiume, "Interactive display and animation of b-spline solids as muscle shape primitives," in *Computer Animation and Simulation '97*, pp. 81–97, Springer-Verlag/Wien, 1997.